SCIENCE CHINA
Technological Sciences

• Article •

August 2016 Vol.59 No.8: 1156–1166
doi: 10.1007/s11431-016-6072-8

Robust segmentation of raw point clouds into consistent surfaces

LIU Yu*

School of Aerospace Engineering, Xiamen University, Xiamen 361005, China

Received December 22, 2015; accepted March 29, 2016; published online July 11, 2016

This paper presents a region-based method for extraction of consistent surfaces from raw point clouds. The method uses a new robust estimation method of constructing seed regions and a new method of orientating regions or surfaces. The robust estimation method selects good seed regions from candidate regions generated randomly in a structured neighborhood. The orientation method uses transition vectors from which include angles of adjacent normal vectors are not greater than 90° and thus can be orientated correctly crossing sharp features or close-by opposite surfaces. The region-based method consists of two levels of segmentation: planar segmentation and quadric segmentation, both of which produce consistent surfaces. The quadric segmentation fits general quadrics by 3 L fitting algorithm in its region growing process and can take consistent planar surfaces as initials. Experimental results show that the robust estimation method has higher probability of success than the traditional one and the orientation method works well. Experimental results also demonstrate the applicability of our method to various data.

raw point clouds, robust estimation, segmentation, orientation, surface reconstruction

Citation: Liu Y. Robust segmentation of raw point clouds into consistent surfaces. Sci China Tech Sci, 2016, 59: 1156–1166, doi: 10.1007/s11431-016-6072-8

1 Introduction

Segmentation is a necessary process in applications such as object recognition [1], modeling [2], compression [3], collision detection [4], and so on. The growing interest in this topic is due to the increasing availability of image, vision and point cloud data. Typically acquired by a laser scanner, the raw point cloud is often incomplete, noisy, non-uniformly sampled, and lacking inherent structure or orientation information. Although various segmentation methods have been proposed, segmentation of raw point clouds is still a challenging problem due to lack of the structures or the mathematical model of the input data, geometry shape complexity and noise (outliers), and newly arisen applications [5–7].

In this paper, we introduce a multi-level method for dividing raw point clouds into consistent surfaces. We denote our method by MCS method since Multi-order Consistent Surfaces are extracted by our method. The MCS method consists of planar segmentation and quadric segmentation. For the planar segmentation, seed regions are constructed by a neighborhood random sample (NRS) method which is a new version of robust estimation techniques [8] by integrating a structured neighborhood. The NRS method intends to fit a surface to points that may contain outliers or be sampled from different surfaces. Compared with the random sample (RS) method used in [9], the NRS method shows high probability of success in determining good regions each of which consists of points only sampled from a single surface. The NRS method lets our region-based method get a seed region just sampled from a single surface as possible instead of a seed region crossing boundaries of different surfaces. The robust estimation method also produces seed region excluding outliers. Starting from a seed region, a region growing process is carried out by a fitting and conquering strategy and adds points as many as possible instead

*Corresponding author (email: mseliuyu@xmu.edu.cn)

of one by one in each iteration.

In order to obtain consistent planar surfaces, we introduce transition vectors ($\boldsymbol{n}_t$ shown in Figure 1(c) and (d)) along border points for transferring orientation information between surfaces. The method via normal propagation [10] is widely applied for orientating normal vectors. Starting from a seed point, it flips inconsistent normal directions between close-by points using a minimum spanning tree (MST) with edge lengths defined by variations in the normal directions. However, propagation errors occur in the presence of sharp features or close-by opposite surfaces [11,12] (shown in Figure 1(a) and (b)). The transition vector aided (TVA) method overcomes the shortness of the conventional approach in a simple way. Moreover, the TVA method transfers orientation information surface by surface instead of point by point.

The quadric segmentation takes outputs of the planar segmentation as initials. Based on consistent orientations of planar surfaces, the quadric segmentation produces consistent quadric surfaces. We fit general quadric surfaces in the quadric segmentation since these surfaces can be well approximated from point clouds with linear cost of the computation through the 3 L fitting algorithm [13]. Figure 2 shows regions and surfaces obtained by the MCS method from the noisy point cloud of the Fandisk model, where points of regions are rendered for clarity.

The remainder of this paper is organized as follows. Section 2 reviews related work on segmentation and normal vector orientation of point clouds. Section 3 introduces the neighborhood random sample method. Section 4 presents transition vectors and corresponding method of getting consistent orientations. Section 5 details the MCS method which uses methods introduced in Sections 3 and 4. Experimental results are given in Section 6. Finally, conclusions are given in Section 7.

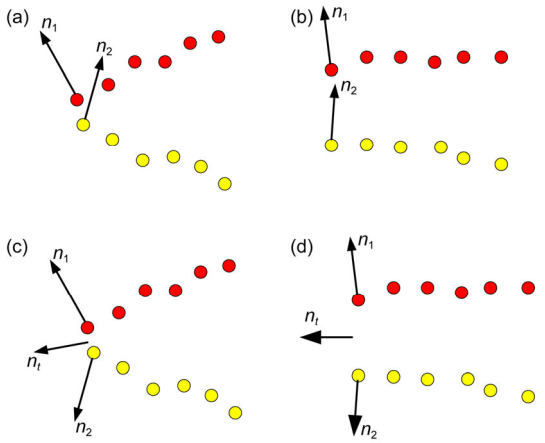

Figure 1 (Color online) Conventional method keeping normal vectors as parallel as possible fails in the presence of (a) sharp features or (b) close-by opposite surfaces, while right results as shown in (c) and (d) are obtained with the aid of the transition vector $\boldsymbol{n}_t$.

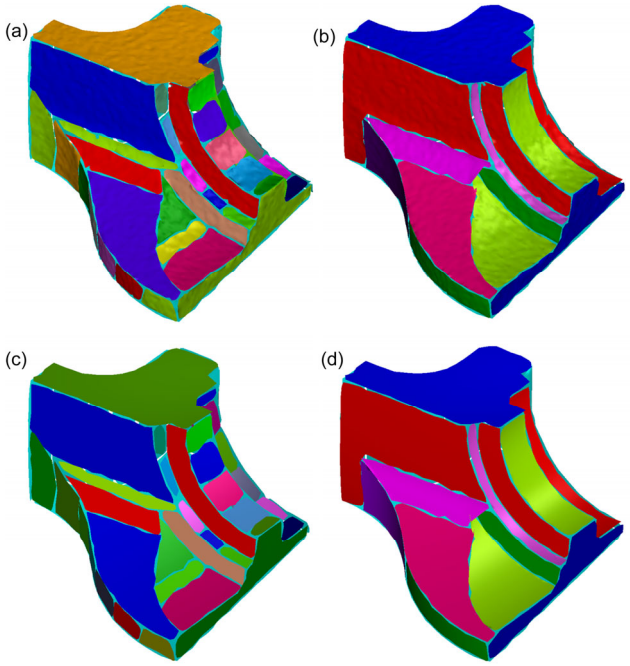

Figure 2 (Color online) Regions and surfaces obtained by the MCS method from the noisy point cloud of the Fandisk model: (a) and (c) are regions and surfaces obtained by planar segmentation respectively; (b) and (d) are regions and surfaces obtained by quadric segmentation respectively.

2 Related work

2.1 Segmentation

Many segmentation methods have been reported, which fall into three categories: edge-based, region-based, and hybrid. Edge-based methods detect edges [14] or critical points [15] separating different regions. Due to the sensitivity to noise and the local characteristic of normal or curvature estimation, edge-based methods are sensitive to noise, and suffer from edge fragmentation and the need for efficient post processing, e.g. gap filling. Using global information such as the homogeneity or similarity of surface properties, region-based methods are more robust to noise than edge-based ones. Normal vectors [16], curvatures [17], color information [18], special structures of the input data (such as scan lines [19] and triangle meshes [20]), and so on, can all be used for finding surface properties. There are some demerits of region-based methods, including that the possibility of over or under-segmentation, the difficulty to localize region borders accurately, and the sensitivity to the choice of the initial seed regions. In order to overcome the limitations involved in edge- and region-based methods, hybrid methods have been developed by combining the edge- and region-based information. For example, points of edges, defective zones and regular regions are identified in [21] using the smoothness indicator, shape index and flatness index which are constructed from local estimated curvatures.

Clustering methods are applied for region extracting and merging [16,22–25]. A drawback of using *k*-means clustering method is that the number of regions is assumed to be known a priori [22,23], while using mean shift method overcomes such drawback [24,25]. Other methods used for region extracting include surface fitting and growing method [17], 3D-grid method [7], Hough transform [26], RANSAC [27], genetic algorithm (GA) [28], and so on. Hough transform is usually used to detect lines in 2D and planes in 3D [26]. RANSAC is a robust method for robust fitting and has been used to detect planes, spheres, cylinders, cones, and tori from noisy point clouds [27]. A drawback of GA-based methods is the difficulty in setting many parameters which must be empirically and carefully determined to avoid premature convergence. Since conventional engineering objects are usually bounded by primitive surfaces, specific segmentation methods for CAD objects are developed in [29,30]. Recently, several planar segmentation methods are also introduced for processing indoor scenes [31] and building roofs [32].

Most of existing segmentation methods rely on specific information such as inside/outside information or consistent surface normal vectors, or that they require the input point cloud is defective free, has less noise (outliers), or is a structured one such as range image or triangle mesh. As demonstrated by Chen et al. [33], the segmentation problem is still not solved even for simple scenes containing only polyhedral objects.

2.2 Point cloud orientation

Consistently oriented normal vectors are necessary for the state-of-the-art reconstruction algorithms [34,35] to produce high quality results. It is difficult for the consistent normal orientation from a point cloud in presence of sharp features, close-by opposite surfaces, data defects, and so on. The existing work in the literature can be classified into two major groups: propagation and non-propagation. The widely used propagation method [10] spreads orientation information from a seed point along the shortest path of a MST with edge lengths defined by variations in the normal directions. The method keeps normal vectors as parallel as possible and fails in the presence of sharp features or close-by opposite surfaces. Some variants using a MST have been introduced by driving normal propagation with different edge measure. In [12], harmonic functions defined on point clouds are used to assign edge weights of a MST. However, harmonic functions fail in areas of critical regions. Huang et al. [11] defines a distance between points to prioritize normal propagation. The distance combines variations in the normal directions and the point coordinates. Although such distance can avoid propagation between points residing on close-by opposite surfaces, it cannot handle the sharp feature with a convex crease even if it uses a detection mechanism for sharp features.

Non-propagation methods are based on volumetric representations or underlying surfaces of point clouds. In [36], an octree is used to represent the pace of point clouds by cells whose corners are associated with in/out tags determined by a visibility checking method. However, a corner is tagged as out with only one view with respective to point clouds. In [37], normal vectors of triangular meshes roughly representing underlying surfaces are used to orientate original point clouds. The triangular meshes are generated through an adaptive spherical cover of point clouds which results in degenerated reconstruction on thick structures and data with heavy noises. In [5], point clouds are shrunk via constrained Laplacian smoothing. Then point clouds are orientated by the visibility checking of the shrunk and the input points. Recently, a method [38] is introduced that estimates normal vectors through a WPA model with both distance and normal variation weights and transfers orientation information from one or more sources. However, the method cannot handle flat models well in experiments.

3 NRS method

We introduce NRS method to construct a good seed region which consists of points sampled from a single surface and considers points sampled from other surfaces as outliers. Assume the neighborhood of a point on a surface consists of points whose distances to the point are not greater than a given constant. The NRS method takes into account the fact that there always exists a neighborhood of a point in a surface (not on boundaries of the surface) that the neighborhood only contains points sampled from the surface. Farther from the point to boundaries of the surface, bigger such neighborhood could be found.

Let d be the farthest distance from a point $\boldsymbol{p}$ to its k nearest neighbors. As shown in Figure 3(a), the region $R_{S1\pm d}$ consists of points whose absolute distances to the surface S_1 are not greater than d and is bounded by two surfaces which are obtained by offsetting the surface S_1 by distances $\pm d$. If $\boldsymbol{p}$ is a point sampled from the surface S_2 and lies in $R_{S1\pm d}$, then it is most possible that the k nearest neighbors of $\boldsymbol{p}$ contain points sampled from both surfaces S_1 and S_2. In fact, the points whose k nearest neighbors are sampled from both surfaces S_1 and S_2 are always included in the region $R_{S1\pm d} \cap R_{S2\pm d}$ as shown in Figure 3(b). In other words, it is most possible that the k nearest neighbors of $\boldsymbol{p}$ only contain points sampled from a single surface if $\boldsymbol{p} \notin R_{S1\pm d} \cap R_{S2\pm d}$.

Based on the above intuitions, the NRS method divides $n=mk$ nearest neighbors of a seed point $\boldsymbol{p}$ into m subsets based on distances from the neighbors to the point $\boldsymbol{p}$. The number of neighbors in each subset is k. The m subsets are separated by concentric circles in 2D (dashed circles shown in Figure 3(c) and (d)) or concentric spheres in 3D. And a candidate point $\boldsymbol{q}$ (shown in Figure 3(d)) is selected at random from each subset. Then the k nearest neighbors (points

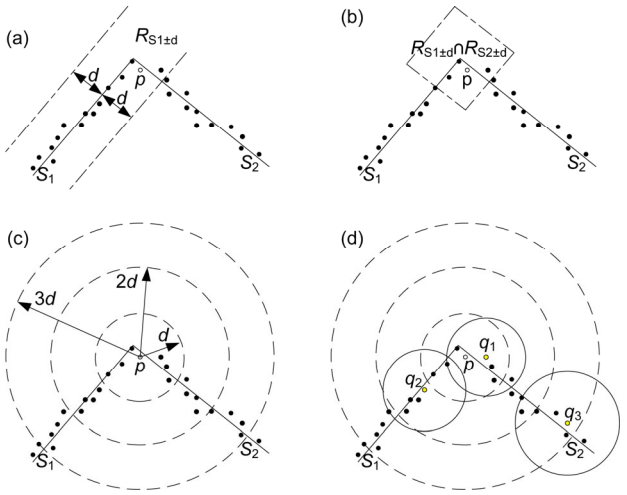

Figure 3 (a) The region $R_{S1\pm d}$ consists of points whose absolute distances to the surface S_1 are not greater than d; (b) the region $R_{S1\pm d} \cap R_{S2\pm d}$ consists of points whose absolute distances to both surfaces S_1 and S_2 are not greater than d; (c) neighbors of a seed point $\boldsymbol{p}$ (denoted by an empty circle) are separated by concentric circles in 2D (dashed circles); (d) three candidate points are selected at random from points in three areas separated by three dashed circles all centered at the seed point $\boldsymbol{p}$. Three candidate seed regions are specified as points in three solid line circles centered at three candidate points.

in solid line circles in Figure 3(d)) of a candidate point are selected to form a candidate seed region. Total m candidate seed regions are obtained finally.

A surface is fitted to each candidate seed region. Residuals of all the neighbors of the seed point $\boldsymbol{p}$ are computed. The residuals are sorted ascending and the lth residual is used to evaluate the candidate seed region. The seed region corresponding to minimal lth residuals is selected as the final seed region. In our experiments, $l = k$ is applied.

Assume P_i (i = 1,⋯, m) is the probability that all of points of the ith candidate seed region are good points belonging to a single surface. Then the NRS method has a probability of success of P = max P_i (i = 1,⋯, m). As indicated by Figure 3(a) and (b), P_i=1 if the ith candidate point $q_i \notin R_{S1\pm d} \cap R_{S2\pm d}$. Such candidate points are points near the seed point $\boldsymbol{p}$ and not in $R_{S1\pm d} \cap R_{S2\pm d}$. As shown in Figure 3(d), the sub-space between circles with radius 2d and 3d does not intersect with $R_{S1\pm d} \cap R_{S2\pm d}$. A candidate seed region generated from any point in such sub-space should have all of their points be good points.

The time complexity of the NRS method is $O(km^2)$. The minimum number k of a seed region is determined by the surface model fitted. Bigger k is required for higher order surfaces.

4 TVA method

Assume there are regions each of which is approximated by a single surface. The task is to define consistent orientations of these surfaces (or regions). The normal propagation keeping normal vectors as parallel as possible between two close-by points implies that the underlying curves in 2D are approximated by two lines S_1 and S_2 in the form shown in Figure 4(a). Although a point and a normal vector at the point are enough for defining a line, but these are insufficient for defining the underlying curves. A line is unbounded and the part of the line to define the underlying curves is not clear. Figure 4(b) shows another possibility that the underlying curves are approximated by the two lines. The normal propagation keeping normal vectors as parallel as possible between two close-by points results in the failure in cases shown in Figure 1(a) and (b).

We introduce transition vectors which give an approximation of the normal vector of the underlying surface between two close-by points. Let $\boldsymbol{p}_1$ and $\boldsymbol{p}_2$ be two close-by points. And assume $\boldsymbol{n}_1$ and $\boldsymbol{n}_2$ are normal vectors at $\boldsymbol{p}_1$ and $\boldsymbol{p}_2$ respectively. Since $\boldsymbol{n}_1$ and $\boldsymbol{n}_2$ may be inconsistent, both $\boldsymbol{n}_{+t}$= ($\boldsymbol{n}_1$ + $\boldsymbol{n}_2$) and $\boldsymbol{n}_{-t}$= ($\boldsymbol{n}_1$ − $\boldsymbol{n}_2$) are possible normal vectors of the underlying surface between $\boldsymbol{p}_1$ and $\boldsymbol{p}_2$. The transition vector $\boldsymbol{n}_t$ between $\boldsymbol{p}_1$ and $\boldsymbol{p}_2$ is selected from $\boldsymbol{n}_{+t}$ and $\boldsymbol{n}_{-t}$ through the size of overlapping areas of underlying surfaces projected along $\boldsymbol{n}_{+t}$ and $\boldsymbol{n}_{-t}$. The overlapping area can be approximated through projecting spheres (or circles in 2D shown in Figure 4 (c) and (d)) centered at each point. Assume $A_{lap}(R_1,R_2,\boldsymbol{n})$ is the overlapping areas of adjacent regions R_1 and R_2 along the direction $\boldsymbol{n}$. Then the goodness of the vectors $\boldsymbol{n}_{+t}$ and $\boldsymbol{n}_{-t}$ are evaluated by $A_{lap}(R_1,R_2,\boldsymbol{n}_{+t})$ and $A_{lap}(R_1,R_2,\boldsymbol{n}_{-t})$ respectively. The vector with the smaller A_{lap} is specified as the transition vector $\boldsymbol{n}_t$. According to the above strategy, the $\boldsymbol{n}_{-t}$ shown in Figure 4(d) should be selected as the transition vector.

One of $\boldsymbol{n}_{+t}$ and $\boldsymbol{n}_{-t}$ constructed in the above process

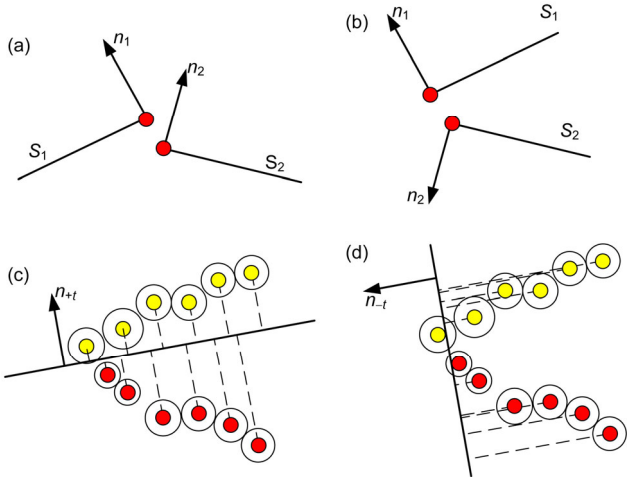

Figure 4 (Color online) Lines in (a) and (b) give two possible definitions of the underling curves using two lines without further information. Considering more points shown in (c) or (d), the definition shown in (b) should be selected. The transition vector $\boldsymbol{n}_{-t}$ shown in (d) instead of $\boldsymbol{n}_{+t}$ shown in (c) is used to select one of possible definitions since the line with normal vector $\boldsymbol{n}_{-t}$ is a better approximation of the underlying curves.

becomes a zero vector if $\boldsymbol{n}_1$ is parallel to $\boldsymbol{n}_2$ (shown in Figure 5 in 2D). We replace the zero vector by a vector perpendicular to the non-zero vector $\boldsymbol{n}_{+t}$ or $\boldsymbol{n}_{-t}$. As shown in Figure 5(c), the $\boldsymbol{n}_{-t}$ is the vector replacing such zero vector and is selected as the transition vector according to overlapping areas. The $\boldsymbol{n}_1$ and $\boldsymbol{n}_2$ shown in Figure 5(a) should be orientated as shown in Figure 5(d).

Vectors $\boldsymbol{n}_1$ and $\boldsymbol{n}_2$ are consistent if they have the same direction relative to $\boldsymbol{n}_t$, i.e. $(\boldsymbol{n}_1 \cdot \boldsymbol{n}_t)(\boldsymbol{n}_2 \cdot \boldsymbol{n}_t)>0$. However, $(\boldsymbol{n}_1 \cdot \boldsymbol{n}_t)(\boldsymbol{n}_2 \cdot \boldsymbol{n}_t)>0$ doesn't work if $\boldsymbol{n}_1$ is parallel to $\boldsymbol{n}_2$ as shown in Figure 5. In fact, the $\boldsymbol{n}_1$ and $\boldsymbol{n}_2$ can be orientated by comparing $A_{lap}(R_1,R_2,\boldsymbol{n}_{+t})$ and $A_{lap}(R_1,R_2,\boldsymbol{n}_{-t})$ without using the $\boldsymbol{n}_t$ explicitly. There are four cases.

1) If $A_{lap}(R_1,R_2,\boldsymbol{n}_{+t})>A_{lap}(R_1,R_2,\boldsymbol{n}_{-t})$, then $\boldsymbol{n}_t = \boldsymbol{n}_{-t}$, and one of $\boldsymbol{n}_1$ and $\boldsymbol{n}_2$ needs to be reversed.

2) If $A_{lap}(R_1,R_2,\boldsymbol{n}_{-t})>A_{lap}(R_1,R_2,\boldsymbol{n}_{+t})$, then $\boldsymbol{n}_t = \boldsymbol{n}_{+t}$, and $\boldsymbol{n}_1$ and $\boldsymbol{n}_2$ have already been consistent.

3) If $A_{lap}(R_1,R_2,\boldsymbol{n}_{-t})=A_{lap}(R_1,R_2,\boldsymbol{n}_{+t})$ and $\boldsymbol{n}_1 \cdot \boldsymbol{n}_2<0$, then one of $\boldsymbol{n}_1$ and $\boldsymbol{n}_2$ needs to be reversed.

4) If $A_{lap}(R_1,R_2,\boldsymbol{n}_{-t})=A_{lap}(R_1,R_2,\boldsymbol{n}_{+t})$ and $\boldsymbol{n}_1 \cdot \boldsymbol{n}_2\geqslant 0$, then $\boldsymbol{n}_1$ and $\boldsymbol{n}_2$ have already been consistent.

In order to orientate two close-by surfaces, the TVA method examines points near their common borders instead of on whole surfaces. The TVA method does not calculate points exactly on common borders of adjacent surfaces. It uses points in a narrow band of borders of corresponding regions. A point of a region lies in narrow bands if at least one of the k nearest neighbors of the point belongs to other regions. Points in narrow bands can also be used to calculate overlapping areas of adjacent surfaces projecting along transition vectors.

The TVA method first selects a seed region at random and fixes its orientation. Then the TVA method propagates orientation information between close-by regions. Along common borders between an inconsistent region and consistent regions, each border point of the inconsistent region is paired with a border point that is the nearest one of the border points of consistent regions. And the inconsistent region is orientated according to the four cases introduced previously. The orientation process is finished until all the regions become consistent.

The cost of computation of the TVA method dependents on the number k_N of nearest neighbors of a paired border point and the number m_N of paired border points. The k_N nearest neighbors can be found by a data structure such as k-d tree. Then the time complexity of the TVA method is $O(m_N k_N \log n)$, where n is the number of input points.

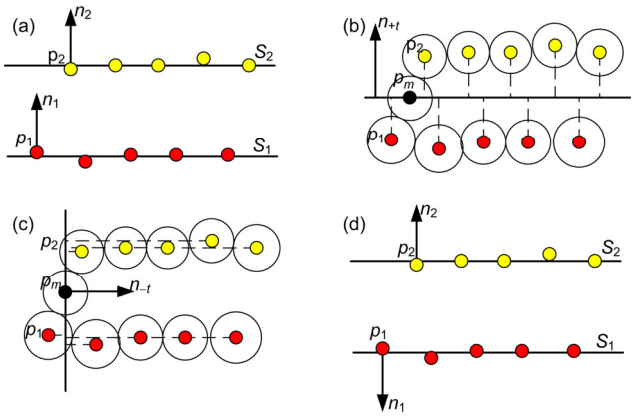

Figure 5 (Color online) Transferring orientation information between two parallel opposite lines: (a) Inconsistent normal directions; (b) and (c) selecting transition vector from two vectors through overlapping areas of projected circles; (d) consistent normal directions.

5 MCS method

The MCS method consists of planar segmentation and quadric segmentation. The planar segmentation uses the NRS method to obtain seed regions, a region growing process to extract planar regions, and the TVA method to orientate planar regions. Planar regions obtained from the planar segmentation are taken as seed regions of the quadric segmentation. Although we can extract consistent quadric surfaces directly from point clouds using the NRS method and the TVA method, starting from planar regions has at least two merits. First, high possibility of success of the NRS method is obtained by specifying few number of points in a seed region since points required for determined a planar surface is smaller than a quadric surface. Second, planar regions can provide an order of extracting quadric surfaces which gives priority for bigger regions. The quadric segmentation starts from the biggest seed region and proceeds according to decent order of the size of planar seed regions. Note that if some points of a planar region have been grouped in the quadric segmentation before the planar region is taken as a seed region, seed region corresponding to the planar region should exclude the grouped points.

Each seed region is expanded through a region growing process which relies on deviations from ungrouped points to a surface fitted to the growing region. The deviation from a point to a plane is specified as the geometric distance from the point to the plane. Geometric distance from a point to a general quadric surface has no closed form solution. For a general quadric surface S_0, the deviation $d(\boldsymbol{p})$ from a point $\boldsymbol{p}$ to S_0 is approximated by the distance from $\boldsymbol{p}$ to a point $\boldsymbol{p}'$ on S_0. The $\boldsymbol{p}'$ is selected as the closer point to $\boldsymbol{p}$ of the two intersection points obtained by intersecting S_0 and the line through $\boldsymbol{p}$ with direction vector $\partial f(\boldsymbol{x})/\partial \boldsymbol{x}|_{\boldsymbol{x}=\boldsymbol{p}}$, where $f(\boldsymbol{x})=0$ is the formula of S_0. Since S_0 is a quadric surface, the $\boldsymbol{p}'$ can be obtained by solving a quadratic equation with one unknown. In the case that the point $\boldsymbol{p}'$ cannot be found, the deviation $d(\boldsymbol{p})$ is replaced by the first order approximation of the real distance from $\boldsymbol{p}$ to S_0 [39].

It is computationally expensive if deviations at all the ungrouped points are calculated. As an alternative, an efficient strategy is to perform work only in a neighborhood of

the growing region. A point of the region lies in the narrow band if at least one of the k nearest neighbors of the point is an ungrouped point. Let $\boldsymbol{p}$ be a point in the narrow band and $\boldsymbol{q}_1$, ⋯, $\boldsymbol{q}_k$ be its k nearest neighbors. And assume $\boldsymbol{q}_1$,⋯, $\boldsymbol{q}_k$ are ordered ascending according to their distances to $\boldsymbol{p}$. The conditions that $\boldsymbol{q}_i$ ($1\leqslant i\leqslant k$) can be grouped into the current region are that $d(\boldsymbol{q}_j)\leqslant\varepsilon$ ($1\leqslant j\leqslant i$), where ε is the threshold of maximal tolerated residual and $d(\boldsymbol{q}_j)$ is the deviation from $\boldsymbol{q}_j$ to the surface fitted to the current region. Such conditions require points closer to $\boldsymbol{p}$ than $\boldsymbol{q}_i$ have been in the current region or can be grouped into the current region. Such condition is originated from the observation that a region should not be separated by points not belonging to the region. After all neighbors of points in the narrow band are examined, an iteration of the region growing process is finished. If no more points can be grouped, the region growing process is ended and the MCS method finds another seed region from ungrouped points to start a new region growing process. Otherwise, the MCS method increases current region, fits surfaces to increased region, and goes into the next iteration of the region growing process. Examining k nearest neighbors of points in the narrow band of the growing region can group a set of points in one time. If there are still ungrouped points after all possible seed regions have been dealt with, these points are identified as outliers.

The general quadric surface fitted in the quadric segmentation is given by $S_0=\{\boldsymbol{x}=(x,y,z)^{\mathrm{T}}|\, f(x,y,z)=0\}$, where $f(x,y,z)=\sum_{i,j,k\geqslant 0,\ i+j+k\leqslant 2} a_{ijk}x^iy^jz^k=\boldsymbol{m}^{\mathrm{T}}\boldsymbol{a}$, $\boldsymbol{m}$ is the vector of monomials, $\boldsymbol{a}$ is the polynomial coefficient vector, and the superscript T denotes the matrix transposition. The surface S_0 is fitted by the 3L fitting algorithm introduced in [13]. Normal vectors required by the 3L fitting algorithm are unknown for raw point clouds. At the beginning of the region growing process, normal vectors at points of a seed region are estimated by normal vectors of the initial surface fitted to the seed region. In following iterations of the region growing process, normal vectors at points of a region are estimated by normal vectors of the surface fitted to the region in the previous iteration.

The MCS method is a multi-order segmentation method. If point clouds are sampled from planes, then the planar segmentation is enough. If point clouds are sampled from higher order surfaces, then the quadric segmentation is necessary. If a smooth surface can't be well approximated by a single quadric surface, it will be represented by two or more quadric surfaces through the quadric segmentation. Therefore many quadric patches may be produced from a model consisting of free form surfaces. And the model can be approximated by combining quadric patch through a Poisson surface [34] or a point set surface (PSS) [40].

The time complexity of the MCS method is determined by the cost of computation of planar segmentation and quadric segmentation. The time complexity of the planar segmentation is determined by the cost of seed region construction and region growing process. A model that is represented by more number of planar surfaces consumes more cost of computation since the seed region construction and region growing process need to be carried out for planar surfaces one by one. The cost of computation of the planar segmentation also increases with the number of points of the input. More number of iterations of the region growing process is usually required for a region containing more number of points. The cost of the seed region construction of the quadric segmentation is relative low since it takes outputs of the planar segmentation as initials. The cost of computation spent on the region growing process of the quadric segmentation is similar with that of the planar segmentation.

6 Experiments

The MCS method has been implemented in MATLAB. All the experiments in this paper are carried out on a PC with a single 3.3 GHz Intel processor. Our implementation was tested on a variety of synthetic and raw point clouds.

For a method of constructing seed regions, we quantify the probability of success of the method as a function of the number k of points of a seed region and the number m of candidate seed regions. Uniformly spaced points are sampled from the two planes. For each value of k and m, total 50 uniformly spaced points along the sharp edge formed by the two planes are used as seed points. A seed region at each seed point is selected from m candidate seed regions through the method to be examined. Then total 50 seed regions are constructed. If all the points of a seed region are sampled from a single plane, the seed region is considered as a good region. The percentage r of good regions in the 50 seed regions is calculated. Higher such percentage means higher probability of success of the examined method. A set of the percentage r is obtained by changing k and m. Then a surface is constructed according to points whose x, y, and z coordinates are k, m, and r respectively. We denote the surface as success rate surface whose height represents the probability of success of a method as a function of the k and the m intuitively.

Figure 6 shows success rate surfaces of our NRS method and the RS method used in [9] on points sampled from two planes with different included angles, where the k changes from 6 to 20, the m changes from 10 to 100, and both methods fit planar surfaces to candidate seed regions. As shown by Figure 6, the probability of success of the RS method increases with m and deceases with k. The RS method produces low percentage of good regions in the experiments if $k\geqslant 10$. The results of the RS method coincide with the success probability $1-(1-g^k)^m$ given in [8], where g is the probability of selecting a single good point at random. The probability of success of the NRS method is stable and is bigger than that of the RS method. The NRS method produces a hundred percent of good regions in most

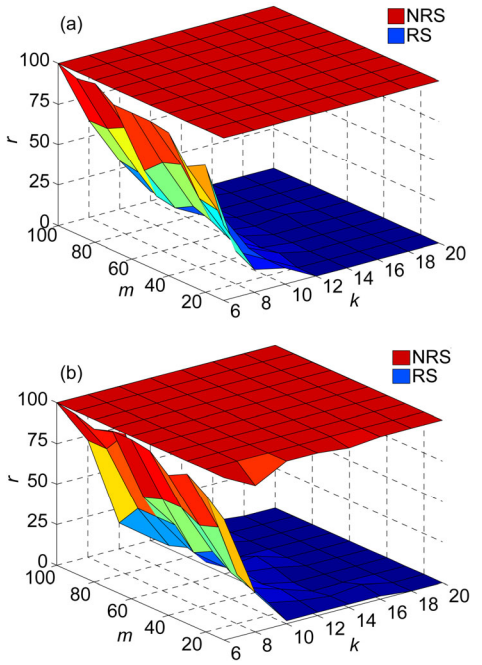

Figure 6 (Color online) The probability of success of the NRS method and the RS method on points sampled from two planes whose included angle is (a) 120 degrees; (b) 60 degrees, where k is the number of points of a seed region, m is the number of candidate seed regions, and r is the percentage of good seed regions. The bigger r means higher probability of success.

cases. Similar results are obtained in the experiments where points are sampled from two planes with other included angles or are contaminated by noises.

For quadric surfaces extracted by the MCS method, we quantify surface reconstruction error as a function of noise and density of points by using a unit sphere as the test shape. Randomly spaced points are sampled from the unit sphere. And the coordinates of the sample points are contaminated by Gaussian noise of zero mean and standard deviation σ to obtain noisy data sets. Then the root-mean-squared (RMS) distance between the ideal and reconstructed spheres is calculated and used as the reconstructed error. The threshold ε of maximal tolerated residual in our region growing process is specified as 3σ in the experiments.

Results in Table 1 of the MCS method shows that RMS error generally increases with decreasing density of points under the same noise level. RMS error also increases with increasing noise on point sets with same number of points. The table does not show results of noiseless point sets since RMS errors under no noise are smaller than 0.000001. Similar results are obtained in the experiments using other quadric surfaces such as cylinders and cones. Compared with results in [41], the proposed method produces a more accurate reconstruction of quadric surfaces from small to very large noise levels. The high accuracy reconstruction can be attributed to the fact that almost all points sampled from a quadric surface are grouped into a single region and

Table 1 RMS error in reconstruction of the unit sphere as a function of the standard deviation of the Gaussian noise σ when using randomly spaced points

# points: σ	0.01	0.03	0.05	0.1
128	0.00222	0.00880	0.01445	0.02941
256	0.00140	0.00562	0.00864	0.00866
1024	0.00072	0.00180	0.00654	0.01051
4096	0.00037	0.00192	0.00392	0.00574
16384	0.00015	0.00072	0.00095	0.00315

are fitted by a single surface in our method. The results also indicate that our segmentation method works well from small to very large noise levels.

Results of the above experiments also provide cues to specify parameters of our method. In the following experiments, both the number k of points of a seed region and the number m of candidate seed regions are specified as 10. The threshold ε of maximal tolerated residual in our region growing process is specified according to noise level. One can fit a small smooth region and measure the largest residual to set the value of ε. Or the ε is specified as half of the average distance from a point to its nearest neighbors on the assumption that the residual of a well sampled point should be not greater than half of the sample interval.

Real data shown in Figure 7 is used in experiments. The points shown in Figure 7(a) are obtained by aligning multi-view scanned points of a laser scanner. The resultant points are noisy and non-uniformly sampled. Due to the specular reflection on planar surfaces of the box part, trips are appeared in the points as shown in the enlarged view of points sampled from the up surface in Figure 7(a). The points shown in Figure 7(b) are obtained by a laser scanner in one set up. The holes of the sheet mental part leave holes in the points. Figure 7(c) shows points sampled from a screwdriver whose cusp is formed by two close planar surfaces. The right of Figure 7(d) shows the points obtained from the inner of a vase. Some points are missing in the inner of the vase since the inner is occluded by the other portion of the vase and cannot be reached by measurement devices such as a laser scanner. Figure 7(e), (f), and (g) are a fish model, a duck model, and a statue model respectively from the AIM@SHAPE shape repository [42].

Figure 8 shows segmentation results of the box, the sheet metal part, the screwdriver, the vase, the fish, the duck, and the statue shown in Figure 7. The first column of Figure 8 is the results obtained from the commercial software: Geomagic Studio which first wraps points into triangle meshes and then extracts regions from triangle meshes. The first column of Figure 8 is obtained by manually adjusting some parameters provided by Geomagic Studio, especially the sensitive parameter of curvatures. Different regions are separated by triangles where high curvatures are detected. In all the results of Geomagic Studio, points near borders aren't grouped into adjacent regions. It is known that curvature

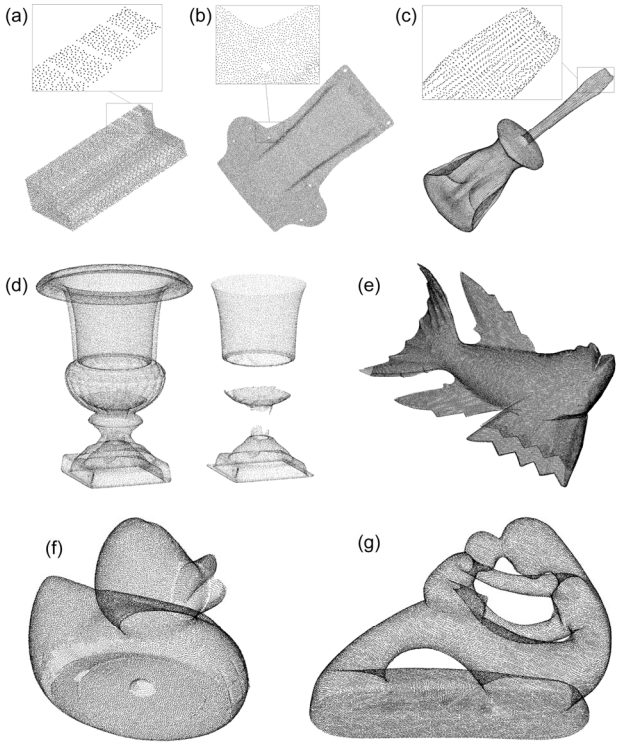

Figure 7 Serval point clouds used in experiments: (a) box part; (b) sheet metal part; (c) screwdriver; (d) vase and its inner; (e) fish; (f) duck; (g) statue.

estimation is sensitive to noises although the triangulation process of Geomagic Studio can smooth out noises. Moreover, it is difficult to select the curvature threshold for curvature-based segmentation. As shown in the first column of Figure 8, the sensitive parameter needs to be increased to separate some smooth connected surfaces (for example the two cylindrical surfaces on the top of the sheet mental part), but a bigger sensitive parameter will divide points sampled from a single surface into several regions (for example the planar surfaces at the base of the vase).

The second and third columns of Figure 8 are results obtained by our planar segmentation and quadric segmentation respectively. Our method directly divides point clouds instead of triangle meshes into different regions. Regions corresponding to planar surfaces are extracted by both the planar segmentation and the quadric segmentation. Regions corresponding to quadric surfaces are divided into many small planar regions by the planar segmentation and are extracted by the quadric segmentation. Compared with Geomagic Studio, our method doesn't need to triangulate point clouds, avoids to produces excessive regions in extracting quadric surfaces, and divides regions and fits surfaces at the same time. As indicated by the results of the fish, the duck, and the statue shown in Figure 8, a smooth surface that can't be well approximated by a single quadric surface will be divided into several quadric surfaces by our method.

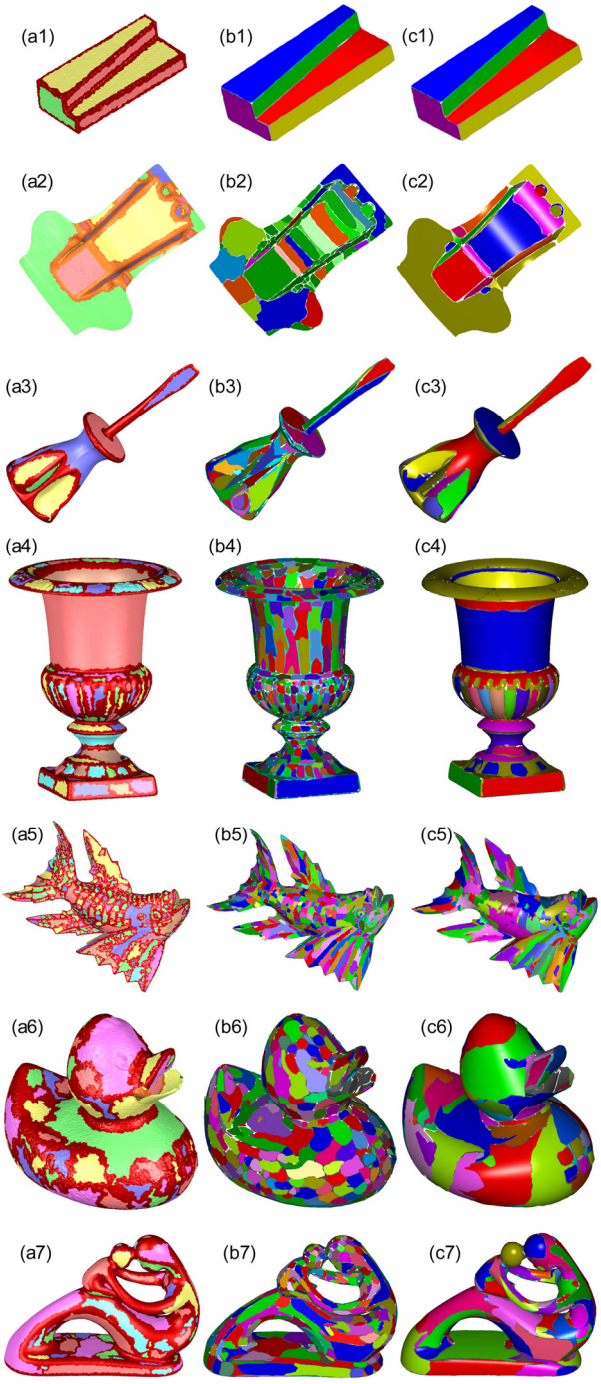

Figure 8 (Color online) Segmentation results of the box, the sheet metal part, the screwdriver, the vase, the fish, the duck, and the statue: (a1)–(a7) are from Geomagic Studio; (b1)–(b7) are from our planar segmentation; (c1)–(c7) are from our quadric segmentation.

Figures 9 and 10 show normal vectors orientated by our method. The box part is an object with sharp features. The sheet metal part is a flat object. The screwdriver and the vase are objects with sharp features and close-by opposite surfaces. Since normal vectors of point clouds are estimated from corresponding surfaces, normal vectors are orientated correctly as long as corresponding surfaces are orientated

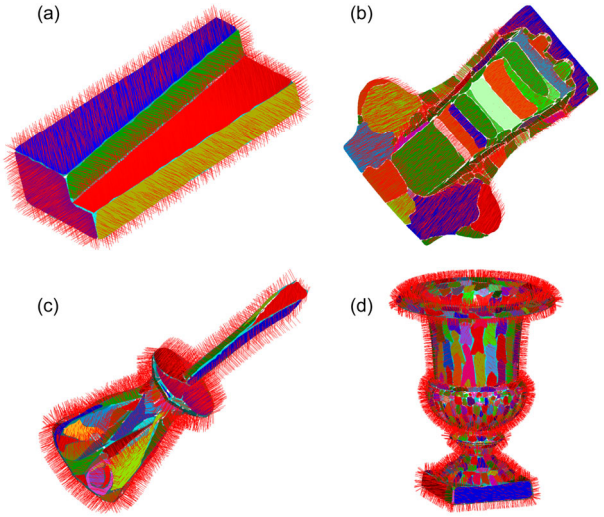

Figure 9 (Color online) Orientated normal vectors in our planar segmentation: (a) box, (b) sheet metal part, (c) screwdriver, (d) vase.

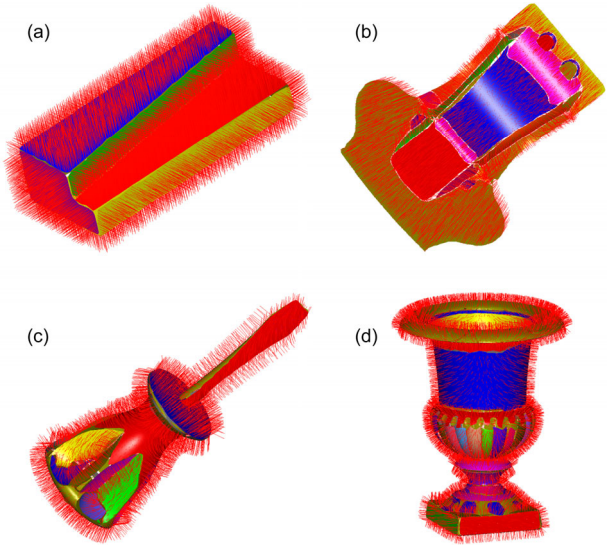

Figure 10 (Color online) Orientated normal vectors in our quadric segmentation: (a) box, (b) sheet metal part, (c) screwdriver, (d) vase.

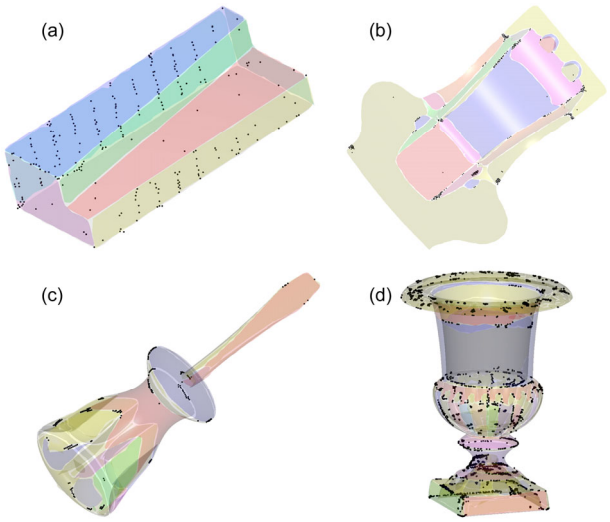

Figure 11 (Color online) Outliers identified from serval real point clouds by our method: (a) box, (b) sheet metal part, (c) screwdriver, (d) vase, where outliers are denoted by black dots and extracted surfaces are plotted transparently.

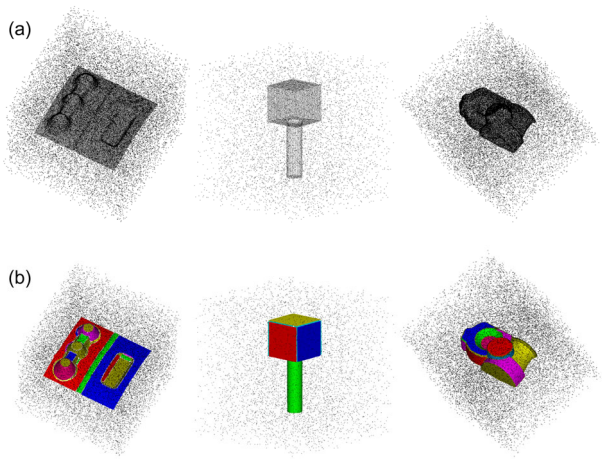

Figure 12 (Color online) Results of our method on point clouds contaminated by 50% outliers. (a) Input point clouds; (b) extracted surfaces and identified outliers.

correctly. Visual checking Figures 9 and 10 indicates that all the normal vectors of these examples are orientated correctly.

Besides points corresponding to surfaces, our method also identifies outliers. Figure 11 shows outliers identified from point clouds of the box, the sheet metal part, the screwdriver, and the vase shown in Figure 7. These outliers consist of points whose distances to extracted surfaces are greater than given threshold ε. We also add outliers to noise point clouds in experiments. The first row of Figure 12 shows point clouds contaminated by 50% outliers, where outliers spread at random in a box containing the original point cloud. The second row of Figure 12 shows extracted surfaces and identified outliers by our method. Figure 12 indicates that our method can reliably extract surfaces from data that contains up to 50% outliers.

To visually demonstrate results under noise, noisy data is obtained by adding Gaussian noise of zero mean and σ=0.1 to original data. Figures 13–15 are the Carter model, the Chinese lion model, and the happy Buddha model respectively from the AIM@SHAPE shape repository [42]. The first row of Figures 13 and 14, and Figure 15(a) show Poisson surfaces using normal vectors estimated by principal component analysis and oriented according to orientation information provided by our method. The second row of Figures 13, 14, and 15(b) show Poisson surfaces over quadric surfaces obtained through our method. The figures demonstrate that Poisson surfaces directly constructed from point clouds preserve surface details but cannot smooth out noise at the same time. And surfaces constructed from

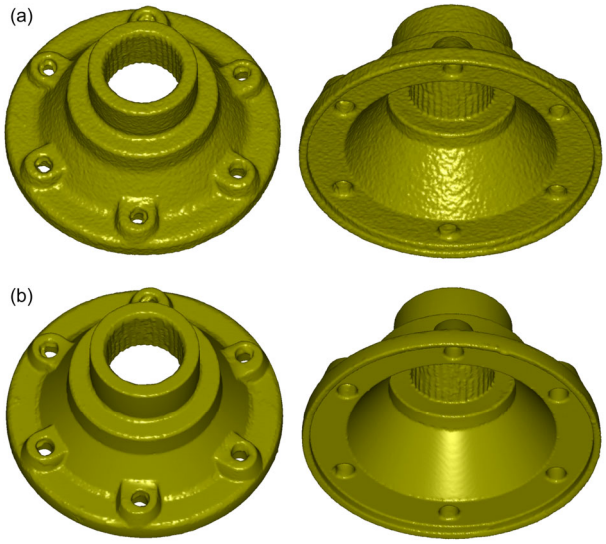

Figure 13 (Color online) Results on noisy data of the Carter model using Poisson surfaces [34]: (a) Poisson over oriented PCA normal; (b) poisson over our quadric surfaces.

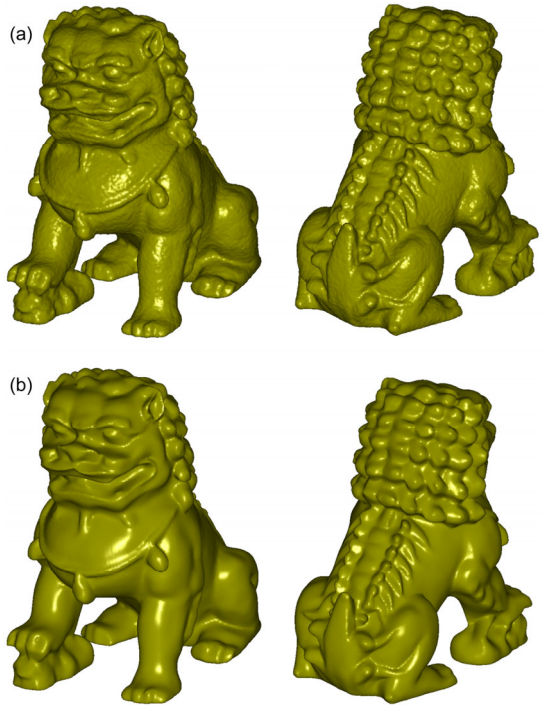

Figure 14 (Color online) Results on noisy data of the Chinese Lion model: (a) Poisson over oriented PCA normal; (b) poisson over our quadric surfaces.

results of our method preserve surface details while smoothing out noise.

7 Conclusion and future work

In this paper, we present a region-based method of extracting consistent surfaces from raw point clouds, which constructs seed regions by the NRS method and orientates directions of regions or surfaces by the TVA method. The NRS method is proposed to select points sampled from a single surface, which treats points sampled from other surfaces as outliers. Compared with traditional RS method, the NRS method shows higher probability of success in determining good regions. The TVA method is proposed to get consistent directions of regions or surfaces with the aided of transition vectors which are intermediate normal vectors constructed between paired boundary points of adjacent regions. The TVA method works well in the presence of sharp features or close-by opposite surfaces.

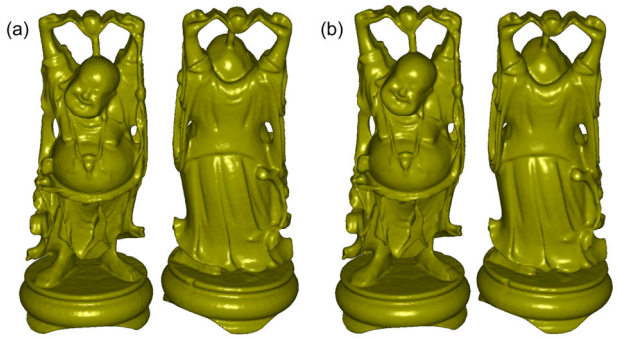

Figure 15 (Color online) Results on noisy data of the happy Buddha model: (a) Poisson over oriented PCA normal; (b) poisson over our quadric surfaces.

The region-based method consists of two levels of segmentation: planar segmentation and quadric segmentation. The segmentation starts from construction of seed regions and proceed by a region growing process. The seed regions are obtained by the NRS method. And planar regions obtained from the planar segmentation can be taken as seed regions of the quadric segmentation, which could decrease the sensitivity to the choice of the initial seed regions of the quadric segmentation. The region growing process uses a fitting and conquering strategy and adds all qualified points in a narrow band of region fronts instead of one by one in each iteration. General quadric surfaces are fitted in the growing process of the quadric segmentation by the 3 L fitting algorithm which produces well approximations of general quadric surfaces and preserve linear cost of the computation simultaneously.

The proposed region-based method only requires coordinates of the input point cloud. It works well in presence of noise and outlier. It identifies outliers as well as different regions. And it produces multi-order consistent surfaces under a given tolerance. In experiments on several raw as well as synthetic point clouds, the proposed method preserves surface details while smoothing noise and can reliably extract surfaces from point clouds that contains up to 50% outliers.

For future work, we would like to speed up the proposed method on multi-core CPUs and explore a GPU-based ac-

celeration. And we are intended to address developing specific procedures to discriminate sharp edges and smooth transitions. Finally, we also see potential in the applications such as shape analysis, surface reconstruction, and so on.

This work was supported by the National Natural Science Foundation of China (Grant No. 51205332), and the SRF for the Returned Overseas Chinese Scholars.

1 Mian A S, Bennamoun M, Owens R. Three-dimensional model-based object recognition and segmentation in cluttered scenes. IEEE T Pattern Anal Mach Intell, 2006, 28: 1584–1601
2 Funkhouser T, Kazhdan M, Shilane P, et al. Modeling by example. ACM T Graphic, 2004, 23: 652–663
3 Karni Z, Gotsman C. Spectral compression of mesh geometry. In: Proceedings of SIGGRAPH, New Orleans, 2000. 279–286
4 Li X, Woon T, Tan T S, et al. Decomposing polygon meshes for interactive applications. In: Proceedings of the ACM Symposium on Interactive 3D Graphics, Venice, 2001. 35–42
5 Cao J, He Y, Li Z, et al. Orienting raw point sets by global contraction and visibility voting. Comput Graph, 2011, 35: 733–740
6 Sheung H, Wang C C L. Robust mesh reconstruction from unoriented noisy points. In: 2009 SIAM/ACM Joint Conference on Geometric and Physical Modeling, San Francisco, 2009. 13–24
7 Vo A V, Truong-Hong L, Laefer D F, et al. Octree-based region growing for point cloud segmentation. ISPRS J Photo Rem Sens, 2015, 104: 88–100
8 Rousseeuw P J, Leroy A M. Robust Regression and Outlier Detection. New York: John Wiley & Sons, 2005
9 Fleishman S, Cohen-Or D, Silva C T. Robust moving least-squares fitting with sharp features. ACM T Graphic, 2005, 24: 544–552
10 Hoppe H, DeRose T, Duchamp T, et al. Surface reconstruction from unorganized points. ACM Siggraph Comput Graph, 1999, 26: 71–78
11 Huang H, Li D, Zhang H, et al. Consolidation of unorganized point clouds for surface reconstruction. ACM T Graphic, 2009, 28: 176
12 Seversky L M, Berger M S, Yin L. Harmonic point cloud orientation. Comput Graph, 2011, 35: 492–499
13 Blane M M, Lei Z, Çivi H, et al. The 3L algorithm for fitting implicit polynomial curves and surfaces to data. IEEE T Pattern Anal Mach Intell, 2000, 22: 298–313
14 Huang J B, Menq C H. Automatic data segmentation for geometric feature extraction from unorganized 3-D coordinate points. IEEE T Robot Autom, 2001, 17: 268–279
15 Berretti S, Del Bimbo A, Pala P. 3D Mesh decomposition using Reeb graphs. Image Vis Comput, 2009, 27: 1540–1554
16 Yamauchi H, Lee S, Lee Y, et al. Feature sensitive mesh segmentation with mean shift. In: 2005 IEEE International Conference on Shape Modeling and Applications, Genova, 2005. 236–243
17 Besl P J, Jain R C. Segmentation through variable-order surface fitting. IEEE T Pattern Anal Mach Intell, 1988, 10: 167–192
18 Zhana Q, Liangb Y, Xiaoa Y. Color-based segmentation of point clouds. Int Arch Photogrammetry, Remote Sens Spat Inf Sci, 2009, 38: 248–252
19 Jiang X Y, Bunke H, Meier U. High-level feature based range image segmentation. Image Vis Comput, 2000, 18: 817–822
20 Yan D M, Wang W, Liu Y, et al. Variational mesh segmentation via quadric surface fitting. Comput-Aided Des, 2012, 44: 1072–1082
21 Di Angelo L, Di Stefano P. Geometric segmentation of 3D scanned surfaces. Comput-Aided Des, 2015, 62: 44–56
22 Cohen-Steiner D, Alliez P, Desbrun M. Variational shape approximation. ACM T Graphic, 2004, 23: 905–914
23 Lavoué G, Dupont F, Baskurt A. A new CAD mesh segmentation method, based on curvature tensor analysis. Comput-Aided Des, 2005, 37: 975–87
24 Liu Y, Xiong Y L. Automatic segmentation of unorganized noisy point clouds based on the Gaussian map. Comput-Aided Des, 2008, 40: 576–594
25 Xiao D, Lin H, Xian C, et al. CAD mesh model segmentation by clustering. Comput Graph, 2011, 35: 685–691
26 Borrmann D, Elseberg J, Lingemann K, et al. The 3D Hough Transform for plane detection in point clouds: A review and a new accumulator design. 3D Res, 2011, 0202: 1–13
27 Schnabel R, Wahl R, Klein R. Efficient RANSAC for point-cloud shape detection. Comput Graph Forum, Blackwell Publishing Ltd, 2007, 26: 214–226
28 Gotardo P F U, Bellon O R P, Boyer K L, et al. Range image segmentation into planar and quadric surfaces using an improved robust estimator and genetic algorithm. IEEE T Syst Man Cy B, 2004, 34: 2303–2316
29 Huang J B, Menq C H. Identification and characterization of regular surfaces from unorganized points by normal sensitivity analysis. J Comput Inf Sci Eng, 2002, 2: 115–24
30 Benkő P, Várady T. Segmentation methods for smooth point regions of conventional engineering objects. Comput-Aided Des, 2004, 36: 511–523
31 Hulik R, Beran V, Spanel M, et al. Fast and accurate plane segmentation in depth maps for indoor scenes. In: 2012 IEEE/RSJ International Conference on Intelligent Robots and Systems, Vilamoura, 2012. 1665–1670
32 Sampath A, Shan J. Segmentation and reconstruction of polyhedral building roofs from aerial lidar point clouds. IEEE T Geosci Remote Sens, 2010, 48: 1554–1567
33 Chen X, Golovinskiy A, Funkhouser T. A benchmark for 3D mesh segmentation. ACM T Graphic, 2009, 28: 73
34 Kazhdan M, Hoppe H. Screened Poisson Surface Reconstruction. ACM T Graphic, 2013, 32: 61–70
35 Ohtake Y, Belyaev A, Seidel H P. A multi-scale approach to 3D scattered data interpolation with compactly supported basis functions. In: 2003 IEEE International Conference on Shape Modeling, Seoul, 2003. 153–161
36 Chen Y L, Chen B Y, Lai S H, et al. Binary orientation trees for volume and surface reconstruction from unoriented point clouds. Comput Graph Forum, Blackwell Publishing Ltd, 2010, 29: 2011–2019
37 Liu S, Wang C C L. Orienting unorganized points for surface reconstruction. Comput Graph, 2010, 34: 209–218
38 Liu J, Cao J, Liu X, et al. Mendable consistent orientation of point clouds. Comput-Aided Des, 2014, 55: 26–36
39 Taubin G. Estimation of planar curves, surfaces, and nonplanar space curves defined by implicit equations with applications to edge and range image segmentation. IEEE T Pattern Anal Mach Intell, 1991, 13: 1115–1138
40 Alexa M, Behr J, Cohen-Or D, et al. Computing and rendering point set surfaces. IEEE T Vis Comput Gr, 2003, 9: 3–15
41 Zagorchev L G, Goshtasby A A. A curvature-adaptive implicit surface reconstruction for irregularly spaced points. IEEE T Vis Comput Gr, 2012, 18: 1460–1473
42 Visualization Virtual Services. Shape Repository Releases. http://visionair.ge.imati.cnr.it/ontologies/shapes/releases.jsp